Journal of Biological Methods | **2014** | Vol. 1(2) | e6
DOI: 10.14440/jbm.2014.26

PROTOCOL

Method for the quantitative measurement of collecting lymphatic vessel contraction in mice

Shan Liao†, Dennis Jones, Gang Cheng‡ and Timothy P. Padera*

Edwin L. Steele Laboratories for Tumor Biology, Department of Radiation Oncology, Massachusetts General Hospital, 55 Fruit St., Boston, MA 02114

*Corresponding author: Timothy P. Padera, Phone: 617-643-6920, Fax: 617-724-5841, E-mail: tpadera@steele.mgh.harvard.edu

†Current Address: Department of Microbiology, Immunology and Infectious Diseases, University of Calgary, Health Sciences Centre, 3330 Hospital Drive NW, Calgary AB T2N 4N1

‡Current Address: Medical Division, Shanghai Roche Pharmaceuticals Ltd., 1100 Long Dong Ave., Pudong District, Shanghai, China 201203

Competing Interests: The authors have declared that no competing interests exist.

Received May 21, 2014; Revision received July 15, 2014; Accepted July 16, 2014; Published July 31, 2014

Abstract Collecting lymphatic vessels are critical for the transport of lymph and its cellular contents to lymph nodes for both immune surveillance and the maintenance of tissue-fluid balance. Collecting lymphatic vessels drive lymph flow by autonomous contraction of smooth muscle cells that cover these vessels. Here we describe methods using intravital microscopy to image and quantify collecting lymphatic vessel contraction in mice. Our methods allow for the measurement of the strength of lymphatic contraction of an individual lymphangion in a mouse, which has not yet been demonstrated using other published methods. The ability to study murine collecting lymphatic vessel contraction—using the methods described here or other recently published techniques—allows the field to dissect the molecular mechanisms controlling lymphatic pumping under normal and pathological conditions using the wide variety of molecular tools and genetic models available in the mouse. We have used our methods to study lymphatic contraction in physiological and inflammatory conditions. The methods described here will facilitate the further study of lymphatic function in other pathological conditions that feature lymphatic complications.

Keywords: lymphatic vessels, lymphatic contraction, intravital imaging, physiology

INTRODUCTION

The initial lymphatic vessels have discontinuous endothelial cell junctions and lack pericyte coverage. These features provide a highly permeable environment that facilitates the collection of extracellular fluid, macromolecules and cells. In contrast to initial lymphatic vessels, the collecting lymphatic endothelial cells are tightly connected by junctional molecules and are covered by smooth muscle cells [2]. Intraluminal valves are anatomically distributed along the collecting lymphatic vessels in order to prevent back flow [3]. The regions between the valves are called lymphangions, which are the functional pumping units of the lymphatic system [4]. Lymphatic smooth muscle cells (SMCs) are highly organized in covering the lymphangion, but are discontinuous over the valves [1]. The contractions of these SMCs drive lymph flow through collecting lymphatic vessels to lymph nodes and, in more proximal lymphatic vessels, propel lymph back to the central circulation. Disruption of lymphatic drainage results in tissue fluid accumulation. Continuous accumulation of fluid may eventually lead to lymphedema—a disfiguring swelling for which there are limited therapies and no cure. Lymphedema carries a huge psychosocial burden and forms conditions for infection of the affected tissue. To understand the molecular regulation of lymphatic function in disease states, it is necessary to have methods to study lymphatic contraction in an animal species with robust molecular and genetic tools available. Here we present an experimental protocol for use in mice to study autonomous lymphatic contraction *in vivo*.

Overview of the technique

The experimental setup for the surgical procedure to study murine autonomous lymphatic contraction is found in **Figure 1** and **Movie S1**, and uses fluorescence microlymphangiography that was originally developed to measure initial lymphatic vessels in humans [5]. We found that the afferent collecting lymphatic vessels to the popliteal lymph node (PLN), which extend from the footpad to the PLN, exhibit consistent lymphatic contraction. Briefly, after administration of anesthesia, we inject 2-3 μl of fluorescent dye subcutaneously into the footpad. Next, we carefully excise a small piece of skin and expose the afferent lymphatic vessels to the PLN (PLVs). The mouse is then transferred to a petri dish and placed onto the stage of an inverted fluorescent microscope to visualize lymphatic contraction. Although we use visible wavelength epifluorescence microscopy to image lymphatic contraction, any high-resolution imaging technique with at least 10 frames per second that can visualize lymphatic vessels can be adapted to these methods, including brightfield videomicroscopy, video-rate multiphoton microscopy [6] and near-infrared epifluorescence imaging [7].

Comparison with other techniques

Lymphatic contraction has been studied in larger animals, such as rat or rabbit. Both *in vivo* and *ex vivo* techniques have been developed and show a critical role for smooth muscle cells in lymphatic contraction [8]. However, limited molecular and genetic tools, as well as few disease models in these species, have prevented further study and the advancement of our understanding of lymphatic contraction. Thus, developing methods to study lymphatic contraction in the mouse is

timely and significant.

In addition to the methods described in this protocol, several groups have recently adapted techniques to image different aspects of lymphatic contraction in mice that were originally developed for larger animals. The two main optical methods adapted to mice with sufficient temporal resolution to measure lymphatic vessel contraction—which excludes many radiographic and magnetic resonance based techniques that can measure other aspects of lymphatic function [9,10]—are *ex vivo* single vessel isolation preparations [11] and non-invasive near-infrared fluorescence imaging [12-15], each with their limitations (**Table 1**). Isolated lymphatic vessel preparations permit high resolution and sharp contrast of the wall of the lymphatic vessel, which can be analyzed to quantify the strength of individual lymphatic contractions (Ejection Fraction) and their frequency [16,17]. Data from isolated vessel experiments in larger animals have yielded great insight into pressure and flow relationships as well as the response of these vessels to pharmacological interventions [16-30]. However, *ex vivo* preparations lack the physiological and molecular cues found *in vivo,* limiting their ability to develop comprehensive models of lymphatic function [31]. The methods we present here for the mouse, similar to other surgical methods to image lymphatic contraction in larger animals [32-34], allow for vessel wall movement and the strength of individual lymphatic contractions to be measured while maintaining the dynamic physiological and molecular environment found *in vivo*.

Using near-infrared fluorescence imaging, which allows deeper imaging in tissue than visible wavelengths, the phasic activity of contracting lymphatic vessels has been studied non-invasively in mice [7,12-15,35]. Near-infrared fluorescence techniques have also been used in humans to study lymphatic drainage and phasic activity in cancer and lymphedema patients [36-38]. This seminal work allows the longitudinal study of lymphatic function, facilitating the evaluation of therapeutic interventions in disease states. Applied to the mouse, longitudinal, large field and non-invasive monitoring is advantageous, highlighted by the ability to show the re-routing of lymphatic drainage in metastatic tumors during disease progression [7]. The non-invasive near-infrared technique can measure the movement of lymph fluid over a distance much larger than a single lymphangion, which is a limitation of the isolated vessel technique and the method presented in this protocol. Interestingly, the frequency of the long-range transport is much slower than the contractions of a lymphangion measured using isolated vessel techniques or the method presented in this protocol. This discrepancy may be potentially explained by the complicated relationship between the contraction of individual lymphangions and the dynamics of intraluminal lymphatic valves that regulate the forward propagation of flow [39,40]. Due to the optical properties of the tissue and skin, measuring the dynamics of the lymphatic vessel wall and ejection fraction is not currently reliable with the non-invasive technique, independent of the optical probe chosen. Light scattering from the overlying skin and tissue distorts the imaged vessel diameter with errors of over 100% at 2 mm of depth and over 1000% at 5 mm of depth for near-infrared optical probes [41]. The use of near-infrared fluorescence can be used in the surgical method described here in order to measure the strength of individual lymphatic contractions, combining the optical advantages of imaging in the near-infrared (e.g. reduced auto-fluorescence) with the ability to resolve vessel wall dynamics. Finally, the ability to study the interaction of cells (e.g. smooth muscle cells, dendritic cells, tumor cells) and the contracting lymphatic vessel has not been demonstrated with the non-invasive near-infrared technique, which is an advantage of the method described in this protocol.

Advantages and limitations

The method presented in this protocol allows for imaging with high spatial and temporal resolution, which permits measurement of lymphatic vessel wall motion over time and allows the study of the interaction between the lymphatic vessel, smooth muscle and immune cells *in vivo*. This method also preserves the *in vivo* context for lymphatic contractions, allowing the effects of nervous system control, systemic molecular regulation and disease processes to be studied. In addition, the vast array of genetic and molecular tools available in mice can be used to dissect molecular mechanisms of lymphatic contraction. However, since this is an acute method, each mouse can only have one imaging session. In addition, surgery may interrupt the connective tissue and may have subtle effects on the lymphatic contraction. In some disease conditions, the lymphatic microenvironment is dramatically changed, including disease processes that cause fibrosis or fat formation. Under these conditions, removing the connective tissue in order to image lymphatic vessels may alter the true function of these vessels. Thus, using all available techniques, including non-invasive near-infrared imaging and isolated vessel preparations, will allow for a robust characterization of lymphatic function (**Table 1**).

Table 1. Comparison of optical techniques with sufficient temporal resolution to measure dynamic lymphatic vessel function.

	Isolated lymphatic vessel	Surgical preparation	Non-invasive imaging
In vivo	No	Yes	Yes
Ability to quantify vessel diameter changes	Yes	Yes	No
Permits longitudinal imaging	No	No	Yes
Able to measure cell interactions	Yes	Yes	No
Ability to accurately control pressure and flow	Yes	No	No
Entire microstructure around vessel remains intact	No	No	Yes
Ability to control molecular concentration around vessels	Yes	No	No

Collecting lymphatic vessels in different tissues have different phenotypic and morphological characteristics [42]. Thus, the mouse PLV may not represent mesenteric or other collecting lymphatic vessels. Furthermore, the molecular mechanisms that govern murine lymphatic contractions may not be the same in humans. Once a molecular understanding is developed and characterized in the mouse PLV, that framework needs to be validated in humans as well as in other anatomical locations. The method presented in this protocol provides a research tool to help drive the discovery that allows us to explore and eventually better understand human lymphatic function, which will require further experimentation.

Although there are many optical imaging options to use with the

surgical method described in this protocol, we will use visible light epifluorescence microscopy in our example due to the simplicity and common availability of the microscopy hardware in biomedical research laboratories, as well as the good reliability of the automated image processing algorithm to analyze data from this simple optical set-up.

Application of the lymphatic contraction model

The molecular and physiological control mechanisms of autonomous lymphatic contraction are just beginning to be uncovered. The methods described here can help further define these control mechanisms and can be used to interrogate theoretical models of lymphatic contraction. For instance, we are developing a theoretical model in which cyclic production of nitric oxide can trigger the smooth muscle cell driven, calcium-dependent lymphatic contractions. We can use the methods described here to test predictions of our model as part of the model validation. As we develop a deeper understanding of the molecular and cellular players involved in autonomous lymphatic contraction, we can use conditional and inducible genetic murine models to intervene in the purported pathways. Furthermore, the availability of transgenic reporter mice that highlight the lymphatic vessels can be utilized to eliminate the need for the lymphangiography injection [43]. We can also use multiple colored labels to highlight different cell types in order to study their interactions in a contracting lymphatic vessel. In this way, the methods described here provide another tool for researchers to develop a robust understanding of autonomous lymphatic vessel contraction.

In addition to studying the physiological control of lymphatic vessel contraction, there is a great need to understand how perturbations in lymphatic contractions may affect lymphatic function in disease states. We have used our model of murine autonomous lymphatic contraction to study the molecular regulation of lymphatic contraction in inflammatory conditions [1]. As we and others have shown, lymphatic function changes in the presence of tumors [7,44-47]. The methods proposed here can be used to further explore how tumors alter lymphatic contraction at the molecular level and if there is any interaction of metastatic tumor cells with collecting lymphatic vessels as they travel to the lymph node. These methods can also be used to dissect the molecular control of lymphatic contractions in a variety of other disease settings in which lymphatic function is altered, including lymphedema, bacterial infection and filariasis.

MATERIALS

Animals

Mice aged 5-6 weeks (either sex can be used): All experiments using mice must be performed in accordance with all institutional and governmental ethics and animal handling requirements.

Reagents (Surgery and dissection reagents)

- ✓ Bacteriostatic 0.9% Sodium Chloride, Injection, USP (Hospira, Inc. cat # 01966-05)
- ✓ Ketamine hydrochloride (100 mg/ml) (Hospira, Inc. cat # 02051-05)
- ✓ Xylazine (100 mg/ml) (Lloyd Laboratories, cat # 139-236)
- ✓ 0.9% Sodium Chloride Irrigation Saline, USP,(Baxter, cat # 2F7124)
- ✓ Sterile Water for Irrigation, USP, (Baxter, cat # 2F7114)
- ✓ 1 ml TB Syringe (Becton, Dickinson and Company, cat# 309659)
- ✓ Polyethylene Tubing 0.28 mm (0.011") O.D. 0.61 mm (0.024") (Intramedic, Becton, Dickinson and Company, cat # 427401)
- ✓ 30G × ½ needle (0.29 mm × 13 mm) (Becton, Dickinson and Company, cat # 304000)
- ✓ Fluorescent dye (2% fluorescein isothiocyanate (FITC)- dextran or rhodamine-dextran), average molecular weight 2,000,000 Da (Sigma Aldrich cat # FD2000S)
- ✓ 100% ethanol (Sigma-Aldrich, cat # E7023)
- ✓ 3" by 3" Cover sponges (Curity/Covidien Inc. cat #1700)
- ✓ Sterile Cell Culture Dish (Corning, cat # 430167) or Petri dish (Becton Dickinson cat # 351005)

Equipment

- ✓ Olympus IX70 Inverted Epi-Fluorescence Microscope
- ✓ Prior Automatic Stage H107P1X
- ✓ Prior OptiScan Motorized Stage System
- ✓ Prior Lumen 200 Fluorescent Illumination System
- ✓ Hamamatsu ORCA-ER Digital Camera
- ✓ Hamamatsu ORCA-ER Camera Controller
- ✓ WIBA and MNG Filter cubes for FITC and Rhodamine visualization, respectively
- ✓ Improvision ORBIT Filter/Shutter Control
- ✓ Olympus 20X 0.40 LCPlanFL Objective
- ✓ Stage Heater (custom-built by Massachusetts General Hospital Machine Shop)
- ✓ Tenma Laboratory DC Power Supply
- ✓ Omega CN132 Autotune Temperature/Process Dual Setpoint Controller
- ✓ Openlab Imaging Software (Perkin Elmer)
- ✓ Surgical tools (Sterilize surgical instruments before the procedure): IRIS scissors (World Precision Instruments (WPI) cat # 500216-G); VANNAS scissors (WPI, cat # 14122-G); IRIS scissors (WPI, cat # 14218-G), forceps Dumont #3 (WPI, cat # 500337); forceps Dumont #5 (WPI, cat # 500233); IRIS Forcep straight (WPI, cat # 15914); IRIS Forcep curved (WPI, cat # 15915)
- ✓ Dissecting Microscope: Nikon SMZ-2T stereomicroscope with Micro Video Instruments Illuminator.
- ✓ Stereomicroscope: Nikon SMZ1500 stereomicroscope with Nikon NI-150 fiber optic illuminator and Nikon Intensilight C-HGFI mercury-fiber illuminator.
- ✓ Injection Apparatus: Connect one end of polyethylene tubing to 30G × ½ needle. Attach a 1ml TB syringe to the needle. Dislodge needle shaft from another 30G × ½ needle. Insert the blunt end of the 30G × ½ needle shaft into the other end of the tubing. The inside diameter of this tubing is 0.28mm. Thus, 1.6 cm of fluid in the tubing is 1 µl. See **Figure S1** and **Movie S1**.

Recipes

- ✓ Ketamine/Xylazine Anesthetic: For 1 ml of anesthetic solution, combine i) 3 ml of 100 mg/ml ketamine hydrochloride, ii) 0.3 ml of 100 mg/ml xylazine and iii) 27 ml of bacteriostatic 0.9% (wt/vol) NaCl. The solution should be freshly prepared before use.
- ✓ Fluorescent Tracer: For 1 ml of FITC-dextran, add 0.02 g FITC-dextran to 1 ml sterile water.
- ✓ 70% Ethanol Solution: To make 10 ml of 70% ethanol, mix 7 ml 100% ethanol with 3 ml sterile water.

PROCEDURE

Surgery to expose afferent lymphatic vessels to the popliteal lymph node (Timing: 20 min)

A visual presentation of the procedure can be found in **Movie S1**.

1. Inject 200 µl ketamine/xylazine intraperitoneally (i.p.) to anesthetize the mouse. Wait until the mouse is completely asleep (about 5 min). Surgery can be performed when the animal no longer reacts to a toe pinch.

   CAUTION: Appropriate permission must be obtained prior to performing animal experiments and surgeries. Multiple strains of mice have been tried using our methods, yielding similar results. The age of the animal is a bigger source of variation so care should be taken to control for mouse age.

2. Inject 2-3 µl 2% FITC-dextran (molecular weight 2,000,000 Da) in PBS subcutaneously into the footpad using the injection apparatus. After filling the entire apparatus with saline, a small air bubble can be introduced in the tip of the injection needle. Then the fluorescent dye can be drawn into the tubing, with the air bubble separating the fluorescent dye and the saline. The distance the air bubble travels and the cross sectional area of the tubing can be used to measure the volume of dye injected. Massage footpad gently to stimulate fluorescent dye uptake.

   TIP: The small amount of liquid is difficult to control using syringe alone, therefore we recommend the use of the injection apparatus.

3. Surgical removal of skin over the lymphatic area: Shave fur from right hind leg. Place the mouse in the prone position, with the lymphatic area facing up (**Fig. 1A**). Place a piece of tape across the footpad. Next, place a piece of tape across the lower abdomen. Wet the hindlimb with 70% ethanol to sterilize the surgical area. Make an incision parallel to the caudal femoral artery and caudal branch of the lateral saphenous vein starting at the ankle of the mouse and directed proximally (**Fig. 1B-C**). Once the incision approaches the popliteal fat pad, make a transverse cut opposite the PLN. The artery, vein and PLVs should be exposed. Remove the flap of skin by making a parallel cut down the leg in the opposite direction of the first incision (**Fig. 1D**). Under the dissecting microscope, ensure that the vessels are clearly exposed.

   TIP: Apply a modest amount of 70% ethanol to skin with fingertips. Spraying ethanol will cause tape to lose adhesiveness, leading to inefficient surgery.

   CAUTION: The lymphatic vessels run parallel with the blood vessels that perfuse the lower leg. Take care not to damage any blood vessel, especially the caudal femoral artery.

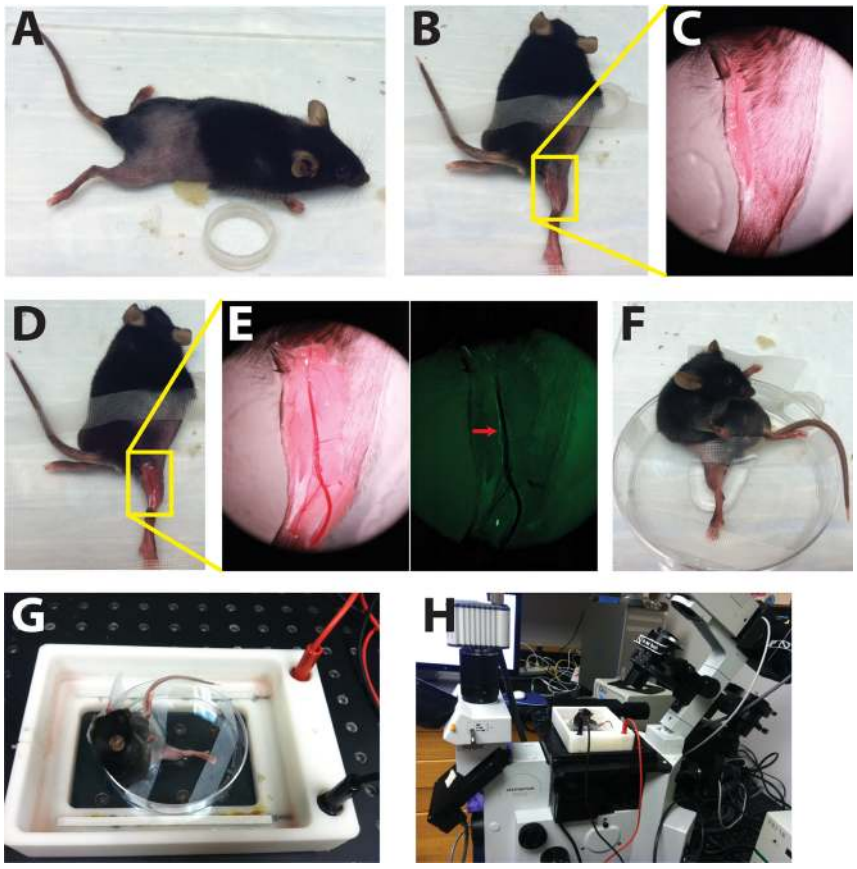

Figure 1: Preparation of mouse to study autonomous collecting lymphatic contraction. A. The hindlimb of the mouse is shaved and placed prone on a heated surface for performing microsurgery. **B.** After immobilizing the mouse with tape and sterilizing the area with 70% ethanol, a small incision is made starting at the back of the ankle and running toward the back of the knee along the medial aspect. **C.** The view through stereomicroscope of incision in (B). **D.** After the PLV is identified, a flap of skin is removed to allow for intravital microscopy. The fat surrounding the PLV is bluntly dissected without damaging any vessels. **E.** The view through the stereomicroscope (left) and a fluorescent view of the PLVs running with the caudal branch of the lateral saphenous vein (right). Red arrow identifies PLV. **F.** The PLV is placed flat against the bottom of a petri dish with the mouse in a "seated" position. Saline is applied to keep the exposed tissue wet. **G.** The mouse and petri dish are placed on a heated stage to maintain the body temperature of the mouse. **H.** The mouse, petri dish and heated stage are placed on the inverted fluorescence microscope.

4. Apply physiological saline solution to hydrate the exposed area.
5. Under the dissecting microscope, cautiously remove fat and connective tissue from around the lymphatic vessels with Dumont #5 forceps and blunt dissection. This improves the optical quality and is needed for high-resolution imaging (**Fig. 1E**). OPTIONAL: The quality of the surgical preparation and fluorescence filling of the PLV can be checked using the stereomicroscope prior to Step 6.

   CAUTION: Do not damage lymphatic vessels. Damage to lymphatic vessels results in loss of contraction and unreliable results.

Preparing the mouse for imaging

6. Place mouse in a 10 cm petri dish. Gently position the exposed lymphatic vessels flatly on the bottom of dish.

   TIP: The leg needs to be in contact against the bottom of the dish; otherwise images of the PLV will not be in focus across the length of the vessel.

7. Place tape across the toes to secure the foot and another piece of tape on the upper thigh to fix the mouse leg in the petri dish. Use a piece of wide tape to support the neck in order to allow the mouse to stay in an upright, seated position (**Fig. 1F**).

   NOTE: Do not tape the footpad or the leg too tightly. This may cause extra pressure and could interrupt the lymphatic contraction. Tape should be loosely applied and the vessel inspected to make sure it is not compressed.

8. Apply 500 µL of NaCl solution to the exposed leg in order to keep the tissue hydrated during the procedure.

   NOTE: The heated stage will cause evaporation of the saline solution. Monitor the level of this solution to prevent dehydration of exposed leg tissue during imaging.

9. Place the petri dish (containing the mouse) in the heating unit to maintain body temperature (**Fig. 1G**).

Intravital imaging (Timing: 75 min)

10. Allow the mouse to rest on stage for 10-15 min (**Fig. 1H**) to stabilize the contractions. Set up microscope to excite and detect FITC fluorescence. The resting period is needed for the vessel to adjust to its dependent position from the prone position during the surgery, to better regulate the temperature and to avoid measuring transients due to the lymphangiography injection.
11. Adjust the focus in order to visualize the lymphatic vessels.
12. Using the imaging software, modify camera contrast levels in order to optimize conditions for later analysis.

    NOTE: High contrast will lead to indiscriminate fluctuations at lymphatic vessel borders, while low contrast may cause background signals to be included in areas selected for quantitation. The full dynamic range of the detection system should be utilized and pixel saturation should be avoided.

13. Observe the lymphatic contractions under the microscope.
14. Acquire time-lapse images for about 30 s. For instance acquire 360 frames at 80 ms/frame (28.8 s). Move stage in order to focus on an adjacent segment of the lymphatic vessel, and take another time-lapse sequence. These will be the two segments recorded for the mouse.

    NOTE: These camera settings can be adapted based on the specific camera available.

15. After 10 min, re-position to focus on each of the prior segments and continue to acquire time-lapse images. Repeat every 10 min for one hour to generate 7 movies per segment to quantify the lymphatic contraction properties of that segment.

    TIP: Animals that have wide variations from the beginning to the end of the imaging session likely have some problem associated with the surgical procedure and should be excluded. We recommend imaging over the course of an hour in order to verify that the pumping is at a steady state and is thus representative of the homeostatic baseline. Of note, in an individual animal, particularly in a pathological state, it is hard to determine whether the lack of lymphatic pumping is due to the disease or the surgical preparation in that animal. Each investigator should establish their failure rate in control animals. One would not expect an experimental failure in every mouse with a pathological process. Using the control failure rate in statistical power calculations allows proper experimental design and group size in order to make appropriate comparisons of the disease state as a group compared to the control state as a group.

16. Save the images for processing.

Timing

The entire protocol should take about 95 min to generate the contraction data. This involves 20 min for the preparation of the PLV model and 75 min for intravital imaging. Image processing occurs off-line and timing will depend on computational speed and number of experiments analyzed.

Image Processing

Our method of lymphatic pumping signal analysis is called the Peak-and-Valley analysis. First we process the time-lapse images of

contracting lymphatic vessels to identify the upper and lower boundaries of the vessel (**Movie S2**) using custom Matlab code (Supplemental Information). We then create plots of the average vessel diameter against time and identify the peaks (maximum diameters when dilated) and valleys (minimum diameters when constricted) in the curve with the algorithm summarized below:

A point is considered a peak/valley if it is the local maxima/minima, and is followed by a diameter measurement of lower/higher value. A user-defined threshold, which is also reviewed by the user after initial processing, is used to identify the size of the required change in order to filter out the noise in the system. Furthermore, peaks and valleys can only appear alternatively in the results. This method robustly identifies peaks and valleys on relatively regular lymphatic pulsing signals as well as noisier signals (**Fig. 2**).

We can then use these data to calculate the contraction frequency, contraction amplitude, ejection fraction and lymph output as described (**Fig. 3**).

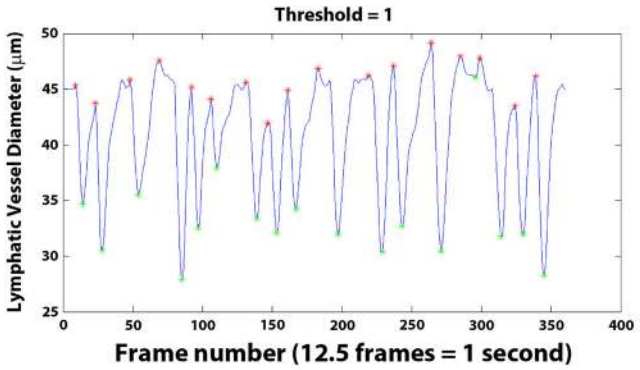

Figure 2. Peak and Valley analysis is able to calculate a representative frequency and amplitude from a noisy sample of lymphatic pulsing as recorded in our study. Blue curve shows the recorded average vessel diameter. Red and green asterisks indicate identified peaks and valleys, respectively.

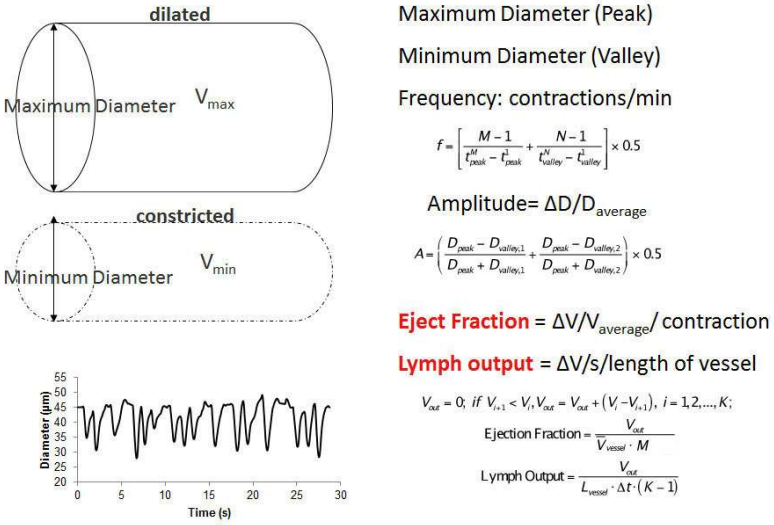

Figure 3. Quantification of lymphatic contraction. Vessel diameters are measured over time and from these measurements we calculate contraction amplitude, contraction frequency, ejection fraction and lymph output. The ejection fraction is a measure of the fraction of fluid that is driven out of the vessel with each contraction. This gives a measure of the strength of lymphatic contraction. The lymph output is a measure of the amount of lymph pumped per time normalized to a unit length of vessel.

Frequency f is calculated as the following:

$$f = \left[\frac{M-1}{t^{M}_{peak} - t^{1}_{peak}} + \frac{N-1}{t^{N}_{valley} - t^{1}_{valley}} \right] \times 0.5 \quad \textbf{(Eqn. 1)}$$

where M and N are respectively the total numbers of peaks and valleys in the signal; t^{1}_{peak} and t^{M}_{peak} are respectively the time when the first and Mth peaks appear; t^{1}_{valley} and t^{N}_{valley} are respectively the time when the first and Nth valleys appear.

We calculate the amplitude as the displacement from the average diameter of the collecting lymphatic vessel. Because the baseline lymphatic diameter is different under each experimental condition, it is more appropriate to compare the relative, instead of absolute, amplitude of the contraction signals. The normalized amplitude from the average diameter A is calculated by the following for each period in the signal:

$$A = \left(\frac{D_{peak} - D_{valley,1}}{D_{peak} + D_{valley,1}} + \frac{D_{peak} - D_{valley,2}}{D_{peak} + D_{valley,2}} \right) \times 0.5 \quad \textbf{(Eqn. 2)}$$

where D_{peak} is the diameter of the peak, $D_{valley,1}$ is the diameter of the preceding valley and $D_{valley,2}$ is the value of the subsequent valley. The value A is then averaged over all the periods in the signal.

We can further estimate the total volumetric fraction of lymph that is pumped by the lymphatic vessel and a theoretical lymph output by integrating the change in vessel volume over all the time steps in the time-lapse movie, assuming that the images are taken at the center of the vessel which is perfectly cylindrical:

$$V_{out} = 0; V_{i+1} < V_i, V_{out} = V_{out} + \left(V_i - V_{i+1}\right), i = 1,2,\ldots,K \quad \textbf{(Eqn. 3)}$$

$$\text{Ejection Fraction} = \frac{V_{out}}{\bar{V}_{vessel} \bullet M} \quad \textbf{(Eqn. 4)}$$

$$\text{Lymph Output} = \frac{V_{out}}{L_{vessel} \bullet \Delta t \bullet \left(K-1\right)} \quad \textbf{(Eqn. 5)}$$

where V_{out} is the total volume of lymph pumped out of the lymphatic vessel during the 30 second movie; K is the number of time steps in the time-lapse movie; $V_i, i = 1,2,\ldots,K$ is the volume of the lymphatic vessel at the ith time step; Δt is the length of each time step; $\bar{V}_{vessel}$ is the time-averaged volume of the lymphatic vessel; M is the total number of peaks in the signal and L_{vessel} is the length of the lymphatic segment. The lymph output is a theoretical value based solely on the vessel wall movement and geometry of the vessel. Based on valve

patency, the status of adjacent lymphangions and other driving forces, actual lymph output may be different. The main utility is to incorporate the frequency component with the strength of lymphatic contraction into a single metric.

ANTICIPATED RESULTS

Typical contractions of the PLV under normal conditions are shown in **Movie S2**. After processing this movie, we obtained the lymphatic contraction profile (**Fig. 2**) and relevant parameters in **Table 3**. The diameter changes between 33 μm to 45 μm and this vessel contracts 36 times per minute. For each contraction, 58% of the volume was ejected (Ejection Fraction) and 469 μm^3 volume is ejected per second normalized to 1 μm of lymphatic vessel length (Lymph Output). Intraluminal collecting lymphatic valves are critical for maintaining unidirectional lymph flow [45]. Using our methods, we are able to visualize the valve motion and study it during disease processes. **Movie S3** shows the typical valve motion during physiological conditions.

The methods to image autonomous lymphatic contraction presented here also permit the study of lymphatic contraction in disease states, with the ability to dissect both cellular and molecular mechanisms. For example, we have transplanted β-actin GFP transgenic mouse bone marrow to a lethally irradiated wild type mouse. After 8 weeks of recovery, we measured lymphatic vessel contraction and their interaction with bone marrow derived cells during physiological and inflammatory conditions. To induce inflammation, 100 μL of 4% oxazolone (Sigma) in acetone was applied topically to all of the skin area surrounding the lower leg, but not touching the skin over the paw.

Under physiologic conditions, there are few bone marrow derived cells adjacent to the lymphatic vessel. However, some bone marrow derived cells appear to directly interact with the lymphatic vessel. Under inflammatory conditions, the strength of lymphatic contraction is inhibited (**Movie S4**) and a large amount of bone marrow derived cells accumulate near the lymphatic vessel (**Fig. 4**). Using the surgical hindlimb method to image lymphatic contraction, one can also resolve cells inside the lymphatic vessels and measure their movement within the vessel.

Table 2. Troubleshooting Table.

Step	Problem	Possible Reason	Solution
2	Lymphangiography injection	Difficulty in controlling the injection volume and force.	Injecting small amounts of liquid in a controlled way is challenging. We recommend using the injection apparatus described in the in the Reagent Setup (Figure S1). After filling the entire apparatus with saline, a small air bubble can be introduced in the tip of the injection needle. Then the fluorescent dye can be drawn into the tubing, with the air bubble separating the fluorescent dye and the saline. The distance the air bubble travels and the cross sectional area of the tubing can be used to measure the volume of dye injected.
		Difficulty in filling the PLV	Subcutaneously inject into the center of the footpad. Injection at the periphery will cause inefficient uptake of FITC-dextran.
3	Cannot locate lymphatic vessels	Unfamiliarity of location of PLV	For beginners, inject Evans Blue dye at the footpad instead of fluorescent dye using the injection apparatus. Lymphatic vessels will be highlighted in blue.
	Trouble immobilizing the leg for the surgery	Dermal tape is not sticking	Apply a modest amount of ethanol to skin with fingertips. Spraying ethanol will cause tape to lose adhesiveness, leading to inefficient surgery.
11	Lymphatic vessels are not clearly visible	Removal of fat is inadequate	Fat tissue may block the fluorescent signal during imaging and distort the optical image. Remove as much fat as possible with Dumont #5 forceps and blunt dissection. (See Step 5)
		Tissue injury during surgery	Make sure that no blood or lymphatic vessels are injured, resulting in blood hemorrhage or damage along the lymphatic vessels.
		Incorrect positioning of leg in petri dish	Make sure the leg is placed against the bottom of the petri dish. This allows for the vessel to remain in focus along its length. (See Step 6).
12	Lymphatic vessel contrast is too faint or too intense.	Volume of injected FITC-dextran was inappropriate.	Use a piece of polyethylene tubing to connect 30G × ½ needle. With this simple device, the injection can be gentle and the small volume can be controlled easily (See Reagent Preparation. Fig. S1).
		Site of injection was inaccurate	Inject into the center of the footpad. Injection at the periphery will cause inefficient uptake of FITC-dextran. (See Step 2).
13	Lymphatic vessels not contracting	Lymphatic vessel damage during surgery.	Overambitious removal of fat or rough handling of the surgical preparation can cause damage to the lymphatic vessels, leading to leakage of FITC-dextran or failure of lymphatic vessels to contract. During surgery, care should be taken not to puncture the lymphatic vessels or move it from its normal position.
		Sub-optimal environment	Wait at least 15 min for mouse to adjust to imaging conditions. Make sure the animal temperature is maintained at 37°C.
		Leg taped too tightly impairing vasculature	Taping the leg too tightly to the petri dish bottom can impair flow. Loosen the tape, while still keeping the PLV flat along the petri dish bottom (See Step 7).

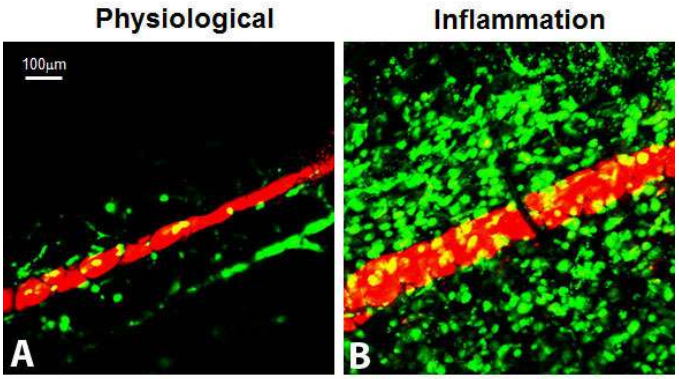

Figure 4. Lethally irradiated C57/Bl6 mice were rescued with bone marrow from a β-actin GFP transgenic mouse. A. Under physiologic conditions there is a modest number of bone marrow derived cells (green) around the PLV (red). **B.** Under inflammatory conditions (four days after oxazolone skin painting), there is a substantial infiltrate of bone marrow derived cells, which are associated with an impairment in lymphatic function (Movie S4). We have shown that *iNOS* expression by bone marrow derived cells contribute to the functional impairment in collecting lymphatic vessels [1].

We found that these bone marrow cells inhibit the lymphatic contraction through expression of *iNOS* and production of nitric oxide. Using a genetically modified mouse deficient in *iNOS*, lymphatic contractions could occur even during inflammation [1]. These results indicate that lymphatic contraction can be impaired during disease processes and the methods presented here allowed the dissection of the molecular and cellular mechanisms. Understanding these and additional molecular mechanisms may lead to new strategies for the treatment of lymphedema and diseases associated with lymphatic impairment.

Table 3. Parameters calculated from Movie S2.

Min diameter (μm)	Max diameter (μm)	Frequency (cpm)	Amplitude (%)	Ejection Fraction (%)	Lymph Output (μm³/s/μm)
33	46	36.3	16	58	469

Acknowledgments

The authors thank Drs. Rakesh K. Jain, Dan G. Duda and Lance L. Munn for their input in the development of this protocol. This work was supported by R00CA137167 (TPP), DP2OD008780 (TPP), R21AI097745 (TPP) and K99HL111343 (SL).

Author contributions

SL developed the initial protocol, performed experiments, analyzed data and contributed to writing the manuscript. DJ performed experiments, analyzed data and contributed to writing the manuscript. GC developed the image analysis software and analyzed data. TPP designed experiments and contributed to writing the manuscript.

References

1. Liao S, Cheng G, Conner DA, Huang Y, Kucherlapati RS, et al. (2011) Impaired lymphatic contraction associated with immunosuppression. Proc Natl Acad Sci U S A 108: 18784-18789. doi: 10.1073/pnas.1116152108. PMID: 22065738
2. Baluk P, Fuxe J, Hashizume H, Romano T, Lashnits E, et al. (2007) Functionally specialized junctions between endothelial cells of lymphatic vessels. J Exp Med 204: 2349-2362. doi: 10.1084/jem.20062596. PMID: 17846148
3. Schmid-Schönbein GW (1990) Microlymphatics and lymph flow. Physiol Rev 70: 987-1028. PMID: 2217560
4. von der Weid PY, Zawieja DC (2004) Lymphatic smooth muscle: the motor unit of lymph drainage. Int J Biochem Cell Biol 36: 1147-1153. doi: 10.1016/j.biocel.2003.12.008. PMID: 15109561
5. Bollinger A, Jäger K, Sgier F, Seglias J (1981) Fluorescence microlymphography. Circulation 64: 1195-1200. PMID: 6170474
6. Kirkpatrick ND, Chung E, Cook DC, Han X, Gruionu G, et al. (2012) Video-rate resonant scanning multiphoton microscopy: An emerging technique for intravital imaging of the tumor microenvironment. Intravital 1: doi: 10.4161/intv.21557. PMID: 24353926
7. Proulx ST, Luciani P, Christiansen A, Karaman S, Blum KS, et al. (2013) Use of a PEG-conjugated bright near-infrared dye for functional imaging of rerouting of tumor lymphatic drainage after sentinel lymph node metastasis. Biomaterials 34: 5128-5137. doi: 10.1016/j.biomaterials.2013.03.034. PMID: 23566803
8. Zawieja DC (2009) Contractile physiology of lymphatics. Lymphat Res Biol 7: 87-96. doi: 10.1089/lrb.2009.0007. PMID: 19534632
9. Stanton AWB, Modi S, Bennett Britton TM, Purushotham AD, Peters AM, et al. (2008) Lymphatic drainage in the muscle and subcutis of the arm after breast cancer treatment. Breast Cancer Res Treat 117: 549-557. doi: 10.1007/s10549-008-0259-z. PMID: 19052859
10. Notohamiprodjo M, Weiss M, Baumeister RG, Sommer WH, Helck A, et al. (2012) MR lymphangiography at 3.0 T: correlation with lymphoscintigraphy. Radiology 264: 78-87. doi: 10.1148/radiol.12110229. PMID: 22523325
11. Scallan JP, Davis MJ (2013) Genetic removal of basal nitric oxide enhances contractile activity in isolated murine collecting lymphatic vessels. J Physiol 591: 2139-2156. doi: 10.1113/jphysiol.2012.250662. PMID: 23420659
12. Kwon S, Sevick-Muraca EM (2007) Noninvasive quantitative imaging of lymph function in mice. Lymphat Res Biol 5: 219-231. doi: 10.1089/lrb.2007.1013. PMID: 18370912
13. Li J, Ju Y, Bouta EM, Xing L, Wood RW, et al. (2013) Efficacy of B cell depletion therapy for murine joint arthritis flare is associated with increased lymphatic flow. Arthritis Rheum 65: 130-138. doi: 10.1002/art.37709. PMID: 23002006
14. Proulx ST, Luciani P, Derzsi S, Rinderknecht M, Mumprecht V, et al. (2010) Quantitative imaging of lymphatic function with liposomal indocyanine green. Cancer Res 70: 7053-7062. doi: 10.1158/0008-5472.CAN-10-0271. PMID: 20823159
15. Gogineni A, Caunt M, Crow A, Lee CV, Fuh G, et al. (2013) Inhibition of VEGF-C modulates distal lymphatic remodeling and secondary metastasis. PLoS One 8: doi: 10.1371/journal.pone.0068755. PMID: 23874750
16. Gashev AA, Davis MJ, Zawieja DC (2002) Inhibition of the active lymph pump by flow in rat mesenteric lymphatics and thoracic duct. J Physiol 540: 1023-1037. PMID: 11986387
17. Takahashi N, Kawai Y, Ohhashi T (1990) Effects of vasoconstrictive and vasodilative agents on lymphatic smooth muscles in isolated canine thoracic ducts. J Pharmacol Exp Ther 254: 165-170. PMID: 2164089
18. Li X, Mizuno R, Ono N, Ohhashi T (2008) Glucose and glucose transporters regulate lymphatic pump activity through activation of the mitochondrial ATP-sensitive K+ channel. J Physiol Sci 58: 249-261. doi: 10.2170/physiolsci.RP004608. PMID: 18597699
19. Ohhashi T, Kawai Y, Azuma T (1978) The response of lymphatic smooth muscles to vasoactive substances. Pflugers Arch 375: 183-188. PMID: 29277
20. Ohhashi T, Takahashi N (1991) Acetylcholine-induced release of endothelium-derived relaxing factor from lymphatic endothelial cells. Am J Physiol 260: 1172-1178.
21. Ohhashi T, Yokoyama S (1994) Nitric oxide and the lymphatic system. Jpn J Physiol 44: 327-342. PMID: 7869598
22. Davis MJ, Lane MM, Davis AM, Durtschi D, Zawieja DC, et al. (2008) Modulation of lymphatic muscle contractility by the neuropeptide substance P. Am J Physiol Heart Circ Physiol 295: 587-597. doi: 10.1152/ajpheart.01029.2007. PMID: 18539752
23. Davis MJ, Meininger GA, Zawieja DC (1992) Stretch-induced increases in intracellular calcium of isolated vascular smooth muscle cells. Am J Physiol 263: 1292-1299. PMID: 1329564
24. Davis MJ, Scallan JP, Wolpers JH, Muthuchamy M, Gashev AA, et al. (2012) Intrinsic increase in lymphangion muscle contractility in response to elevated afterload. Am J Physiol Heart Circ Physiol 303: 795-808. doi: 10.1152/

ajpheart.01097.2011. PMID: 22886407

25. Gashev AA, Delp MD (2006) Zawieja DC (2006) Inhibition of active lymph pump by simulated microgravity in rats. Am J Physiol Heart Circ Physiol 290: 2295-2308. doi: 10.1152/ajpheart.00260.2005. PMID: 16399874
26. Gashev AA, Zawieja DC (2010) Hydrodynamic regulation of lymphatic transport and the impact of aging. Pathophysiology 17: 277-287. doi: 10.1016/j.pathophys.2009.09.002. PMID: 20226639
27. Scallan JP, Wolpers JH, Muthuchamy M, Zawieja DC, Gashev AA, et al. (2012) Independent and interactive effects of preload and afterload on the pump function of the isolated lymphangion. Am J Physiol Heart Circ Physiol 303: 809-824. doi: 10.1152/ajpheart.01098.2011. PMID: 22865389
28. Zawieja DC, Davis KL (1993) Inhibition of the active lymph pump in rat mesenteric lymphatics by hydrogen peroxide. Lymphology 26: 135-142. PMID: 8258987
29. von der Weid PY, Crowe MJ, Van Helden DF (1996) Endothelium-dependent modulation of pacemaking in lymphatic vessels of the guinea-pig mesentery. J Physiol 493 (Pt 2): 563-575. PMID: 8782117
30. Von_der_Weid PY, Van_Helden DF (1996) Beta-adrenoceptor-mediated hyperpolarization in lymphatic smooth muscle of guinea pig mesentery. Am J Physiol 270: 1687-1695.
31. Benoit JN, Zawieja DC, Goodman AH, Granger HJ (1989) Characterization of intact mesenteric lymphatic pump and its responsiveness to acute edemagenic stress. Am J Physiol 257: 2059-2069. PMID: 2603989
32. Zawieja DC, Greiner ST, Davis KL, Hinds WM, Granger HJ (1991) Reactive oxygen metabolites inhibit spontaneous lymphatic contractions. Am J Physiol 260: 1935-1943. PMID: 2058726
33. Shirasawa Y, Ikomi F (2000) Ohhashi T (2000) Physiological roles of endogenous nitric oxide in lymphatic pump activity of rat mesentery *in vivo*. Am J Physiol Gastrointest Liver Physiol 278: 551-556. PMID: 10762608
34. Wu TF, Carati CJ, Macnaughton WK (2006) von der Weid PY (2006) Contractile activity of lymphatic vessels is altered in the TNBS model of guinea pig ileitis. Am J Physiol Gastrointest Liver Physiol 291: 566-574. doi: 10.1152/ajpgi.00058.2006. PMID: 16675748
35. Robinson HA, Kwon S, Hall MA, Rasmussen JC, Aldrich MB, et al. (2013) Non-invasive optical imaging of the lymphatic vasculature of a mouse. J Vis Exp : doi: 10.3791/4326. PMID: 23524658
36. Sevick-Muraca EM, Sharma R, Rasmussen JC, Marshall MV, Wendt JA, et al. (2008) Imaging of lymph flow in breast cancer patients after microdose administration of a near-infrared fluorophore: feasibility study. Radiology 246: 734-741. doi: 10.1148/radiol.2463070962. PMID: 18223125
37. Adams KE, Rasmussen JC, Darne C, Tan I, Aldrich MB, et al. (2010) Direct evidence of lymphatic function improvement after advanced pneumatic compression device treatment of lymphedema. Biomed Opt Express 1: 114-125. doi: 10.1364/BOE.1.000114. PMID: 21258451
38. Rasmussen JC, Tan IC, Marshall MV, Fife CE, Sevick-Muraca EM (2009) Lymphatic imaging in humans with near-infrared fluorescence. Curr Opin Biotechnol 20: 74-82. doi: 10.1016/j.copbio.2009.01.009. PMID: 19233639
39. Davis MJ, Rahbar E, Gashev AA, Zawieja DC, Moore JE (2011) Determinants of valve gating in collecting lymphatic vessels from rat mesentery. Am J Physiol Heart Circ Physiol 301: 48-60. doi: 10.1152/ajpheart.00133.2011. PMID: 21460194
40. Mellor RH, Brice G, Stanton AWB, French J, Smith A, et al. (2007) Mutations in FOXC2 are strongly associated with primary valve failure in veins of the lower limb. Circulation 115: 1912-1920. doi: 10.1161/CIRCULATIONAHA.106.675348. PMID: 17372167
41. Weiler M, Kassis T, Dixon JB (2012) Sensitivity analysis of near-infrared functional lymphatic imaging. J Biomed Opt 17: 66019. doi: 10.1117/1.JBO.17.6.066019. PMID: 22734775
42. Gashev AA, Davis MJ, Delp MD, Zawieja DC (2004) Regional variations of contractile activity in isolated rat lymphatics. Microcirculation 11: 477-492. doi: 10.1080/10739680490476033. PMID: 15371129
43. Truman LA, Bentley KL, Smith EC, Massaro SA, Gonzalez DG, et al. (2012) ProxTom lymphatic vessel reporter mice reveal Prox1 expression in the adrenal medulla, megakaryocytes, and platelets. Am J Pathol 180: 1715-1725. doi: 10.1016/j.ajpath.2011.12.026. PMID: 22310467
44. Hoshida T, Isaka N, Hagendoorn J, di Tomaso E, Chen Y, et al. (2006) Imaging steps of lymphatic metastasis reveals that vascular endothelial growth factor-C increases metastasis by increasing delivery of cancer cells to lymph nodes: therapeutic implications. Cancer Res 66: 8065-8075. doi: 10.1158/0008-5472.CAN-06-1392. PMID: 16912183
45. Isaka N, Padera TP, Hagendoorn J, Fukumura D, Jain RK (2004) Peritumor lymphatics induced by vascular endothelial growth factor-C exhibit abnormal function. Cancer Res 64: 4400-4404. doi: 10.1158/0008-5472.CAN-04-0752. PMID: 15231646
46. Lahdenranta J, Hagendoorn J, Padera TP, Hoshida T, Nelson G, et al. (2009) Endothelial nitric oxide synthase mediates lymphangiogenesis and lymphatic metastasis. Cancer Res 69: 2801-2808. doi: 10.1158/0008-5472.CAN-08-4051. PMID: 19318557
47. Padera TP, Kadambi A, di Tomaso E, Carreira CM, Brown EB, et al. (2002) Lymphatic metastasis in the absence of functional intratumor lymphatics. Science 296: 1883-1886. doi: 10.1126/science.1071420. PMID: 11976409

Supplementary information

Movie S1. Movie of the experimental procedures described in this Protocol.

Movie S2. Autonomous contraction of the PLV. The edge of the contracting vessel is highlighted in red by the edge-finding algorithm of the image processing and analysis software. Scale bar=25 μm.

Movie S3. Intraluminal valve motion is visible during lymphatic contraction. Scale bar=25 μm.

Movie S4. Lymphatic contraction is severely impaired along with PLV dilation during inflammation. The edge of the vessel is highlighted in red by the edge-finding algorithm of the image processing and analysis software. Scale bar=25 μm.

Additional supplementary information of this article can be found online at http://www/jbmethods.org.